PROCEEDINGS, 41st Workshop on Geothermal Reservoir Engineering
Stanford University, Stanford, California, February 22-24, 2016
SGP-TR-209

Modeling Heat Flow in the Eastern Snake River Plain Aquifer

Mitchell Plummer, Carl D. Palmer, Travis McLing and A. Jeffrey Sondrup

Idaho National Laboratory, P.O. Box 1625, MS2208, Idaho Falls, ID, 83415, USA

Mitchell.Plummer@inl.gov

Keywords: Eastern Snake River Plain, heat flow, viscous dissipation, modeling

ABSTRACT

The Eastern Snake River Plain (ESRP) in southern Idaho is a region with significant potential as a geothermal energy resource. Deep boreholes in the region suggest generally high geothermal heat flux, of approximately 100 mW m^{-2}, with a slight eastward increase across the plain (Blackwell 1989). Evidence of that vertical heat flux, however, is largely masked by the rapid flow of cold groundwater that originates in the Yellowstone Plateau and transports heat horizontally through the highly permeable basalts making up the aquifer. This masking means that spatial distribution of temperature and heat flux below the aquifer is only poorly known and that, in turn, reduces confidence in identification of areas most suitable for geothermal development.

To improve understanding of temperature distribution below the aquifer and advance the general understanding of heat flux in the ESRP, we conducted groundwater heat transport simulations and compared results to mapped groundwater temperatures. Our heat transport model utilizes the groundwater flow model developed by the Eastern Snake Plain Hydrologic Modeling Committee, a MODFLOW-based model that has been well tested and calibrated for resource management. Heat flow was simulated using the MT3DMS software package that is compatible with MODFLOW. The model accounts for basal heat flow, conductive loss of heat from top of the aquifer through the vadose zone, and advective addition of heat through rivers, precipitation, irrigation, and injection wells.

Simulations with constant basal heat flow capture many of the salient features of the measured temperature distribution. Results demonstrate the relative importance of advective transport in the aquifer. Viscous dissipation has been shown to be significant in the aquifer and that thermal input is being added to the model. The model is being calibrated against measured temperature profiles and heat flow measurements that have been taken below the aquifer. These vertical temperature profiles can also provide information about groundwater flux and mechanical dispersion within the aquifer.

1. INTRODUCTION

The Eastern Snake River Plain (ESRP) in southern Idaho is a region with significant potential as a geothermal energy resource. Deep boreholes in the region suggest a systematic eastward increase in heat flow from about 75-90 mW m^{-2} to 90-110 mW m^{-2} across the plain (Blackwell 1989). However, evidence of that heat flux is largely masked by the rapid flow of cold groundwater originating in the Yellowstone Plateau though the highly permeable basalts making up the aquifer. This masking means that spatial distribution of temperature and heat flux below the aquifer is only poorly known making identification of drilling sites with high thermal gradients difficult and potentially increasing the risk for geothermal exploration.

To improve understanding of temperature distribution below the aquifer and advance the general understanding of heat flux in the ESRP, we conducted a groundwater heat transport simulation. This study is aimed at estimation of sub-aquifer heat flux by adjustments to match groundwater temperature. We have employed the East Snake Plain Aquifer Model (ESPAM) to simulate groundwater flow processes that mask surficial evidence of the deep heat flux. Our approach assumes that groundwater flow directions and rates are relatively well understood in ESPAM, as uncertainties in calculated groundwater temperatures reflect uncertainties in groundwater movement as well as in heat flux boundary conditions. We believe that this is a realistic assumption because the eastern Snake River Plain aquifer is a sole source water supply for much of southeastern Idaho, groundwater flow has been well studied, for decades, by multiple agencies, including the USGS, Idaho Water Resources Research Institute (IWRRI), the Idaho Department of Water Resources (IDWR) and UI. ESPAM (Cosgrove, Contor, and Johnson 2006) was developed and is maintained by the Idaho Department of Water Resources, which has undergone extensive calibration, validation, and uncertainty analysis and continues to be improved for use as a decision making tool for water rights in the ESRP. This document describes the approach that we have taken to simulate heat flow in the Eastern Snake River Plain of Idaho and summarized preliminary results of our simulations.

2. EASTERN SNAKE RIVER PLAIN AQUIFER MODEL

The ESPAM is based on the MODFLOW groundwater flow modeling package and its use and application is widely available. To calculate heat transport effects in ESPAM, we used the MT3DMS transport package, which is readily coupled to MODFLOW through a graphical user interface such as Groundwater Modeling Software (GMS) or Visual Modflow. Through this coupling of MT3DMS to MODFLOW the detailed recharge distribution, groundwater-river interaction, point source/sink distribution associated with wells and springs, and calibrated transmissivity distribution of the ESPAM will be the basis for the heat transport model.

We obtained the MODFLOW files from IWRRI site (https://www.idwr.idaho.gov/waterinformation/projects/espam/). We modified the files so they were in units of meters and days. We were able to get the model to run in both the GMS and the Visual MODFLOW Flex interfaces. The resulting modeled hydraulic head distribution is illustrated in Figure 1.

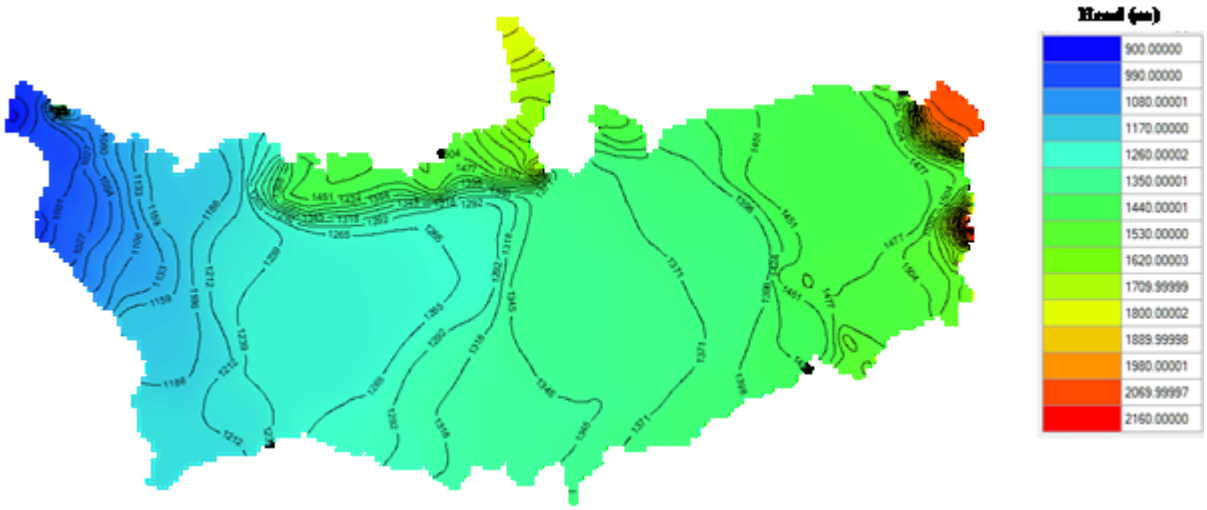

Figure 1. Hydraulic head distributions in the Eastern Snake River Plain computed by the ESRAM

3. MODELING APPROACH

3.1 Heat Transport

To simplify the used of the ESPAM aquifer model as the basis for our heat transport model, we developed it within the MODFLOW family of groundwater models, using MT3DMS to simulate the heat transport. While MT3DMS is designed for simulating solute transport, the similarities in the differential equations for heat flow and solute transport allow us to use MT3DMS if we define parameters and boundary conditions in an appropriate manner. The first step is to substitute the thermal diffusivity for the molecular diffusion coefficient. The sorption of heat by the aquifer matrix is included by using the linear sorption model using a sorption coefficient (K_d) of

$$K_d = \frac{c_s}{\rho_w c_w} \tag{1}$$

where c_w is the specific heat of water (J kg^{-1} °C^{-1}), c_s is the specific heat of the solid matrix (J kg^{-1} °C^{-1}), and ρ_w is the fluid density (kg m^{-3}). The following sections describe how boundary conditions and source/sink terms are handled using MT3DMS.

3.1.1 Advective Heat Flow

Advective heat flow across a boundary can occur under various scenarios but a key one from our perspective is the case of groundwater recharge. Under these conditions, the heat flux, q_h, in J m^{-2} s^{-1} that is advectively transported into an aquifer is

$$q_h = q_{rech} c_w \rho_w T_g \tag{2}$$

where q_{rech} is the recharge rate (L/T) and T_g is the temperature of the ground surface and which could be considered close to the average air temperature. Alternatively, this heat could be added to the model via a fictitious injection well using

$$q_h = Q_r c_w \rho_w T / A \tag{3}$$

where Q_r is the rate of injection (m^3 s^{-1}) and A is the area over which the recharge occurs (e.g., the area of a cell in a finite difference grid). In the ESPAM model, recharge was lumped with irrigation and injection and simulated using wells. However, as discussed in a subsequent section, we use the recharge option to simulate a portion of temperature-dependent heat-flow boundaries.

3.1.2 Specified Heat Flux

For a specified heat flux in J m^{-2} s^{-1} that is conductively transported into an aquifer, there is no direct way of including the boundary because solute transport models require that mass be carried into the system dissolved in a fluid. Nonetheless, this type of boundary condition can be simulated by advecting an equivalent amount of heat by a trivial amount of fluid flow. This idea can be illustrated by considering the energy balance which requires that the conductive heat flux, q_h, be equated to an advective heat flux:

$$q_h = -\lambda_x \frac{\partial T}{\partial x} = q_b c_w \rho_w T \tag{4}$$

where λ_x is the thermal conductivity in the x direction. Using an arbitrarily small value of water flux at the boundary (q_b), the appropriate temperature can then be calculated from

$$T = \frac{q_h}{q_b c_w \rho_w} \tag{5}$$

Temperature-Dependent Diffusive Heat Flow Across a Boundary

For heat loss across a boundary where the temperature on the other side is known (i.e., heat diffusion across the vadose zone), the heat flux can be written as

$$q_h = -\lambda_{vz,z} \frac{\partial T}{\partial z} = -\frac{\lambda_{vz,z}}{b_{vz}} \left(T - T_g \right) \tag{6}$$

(Wood et al., 2007) where b_{vz} is the thickness of the vadose zone, $\lambda_{vz,z}$ is the vertical thermal conductivity of the vadose zone, and T_g is the temperature of the ground surface. Equation (6) can be considered two different terms, $q_{h,1}$ and $q_{h,2}$, where

$$q_{h,1} = -\frac{\lambda_{vz,z}}{b_{vz}} T \tag{7}$$

$$q_{h,2} = \frac{\lambda_{vz,z}}{b_{vz}} T_g \tag{8}$$

Eq. (7) can be converted from mass per unit time across the area of the cell to mass per unit time over the volume of the cell by dividing both sides of equation (7) by the height of the cell (Δz_{cell}) to give

$$\frac{q_{h,1}}{\Delta z_{cell}} = \frac{\partial H}{\partial t} = -\frac{\lambda_{vz,z}}{b_{vz} \Delta z_{cell}} T \tag{9}$$

Substituting $H = \rho_w c_w T$ into Eq. (9) and rearranging terms, yields

$$\frac{\partial T}{\partial t} = -\frac{\lambda_{vz,z}}{b_{vz} \Delta z_{cell} \rho_w c_w} T \tag{10}$$

which has a form of a first-order irreversible reaction equation

$$\frac{\partial C}{\partial t} = -k_s C \tag{11}$$

but with the rate coefficient, k_T, of

$$k_T = \frac{\lambda_{vz,z}}{b_{vz} \Delta z_{cell} \rho_w c_w} \tag{12}$$

This analogy allows us to use the first-order reaction equations included in MT3DMS to represent this heat-loss term.

The second part of Eq. (6) (i.e., Eq. (8)) can be treated either as a recharge term:

$$q_{h,2} = \frac{\lambda_{z,vz}}{b_{vz}} T_g = q_{fr} c_w \rho_w T_{fr} \tag{13}$$

where q_{fr} is a fictitious recharge rate and T_{rf} is the temperature of this recharge. T_{rf} can be calculated from Eq. (33) using the assumed q_{fr} by

$$T_{fr} = \frac{\lambda_{z,vz} T_g}{b_{vz} q_{fr} c_w \rho_w} \tag{14}$$

3.1.3 Viscous Dissipation

A process that is often neglected in modeling heat flow is viscous dissipation. Viscous dissipation is the conversion of mechanical energy of a fluid to heat (Manga and Kirchner, 2004). The mechanical energy of the fluid is the fluid potential (Ψ). In most groundwater systems Ψ (joules kg^{-1}) can be defined as

$$\Psi = gh \tag{15}$$

where g is the acceleration of gravity (9.80665 m s^{-2}) and h is the hydraulic head (m) (e.g., Freeze and Cherry, 1979).

Consider at one-dimensional aquifer system with a hydraulic head drop of Δh, a temperature inflow of T_i and a temperature outflow of T_o. An energy balance of this system requires the energy flowing out of the system (joules s^{-1}) is equal to the energy entering the systems plus the energy gained by the conversion of mechanical energy to heat:

$$\underset{\text{Outflow}}{\theta c_w \rho_w v_x T_o \Delta y \Delta z} = \underset{\text{Inflow}}{\theta c_w \rho_w v_x T_i \Delta y \Delta z} - \underset{\text{ME Conversion}}{\theta v_x \Delta y \Delta z \rho_w g \Delta h} \tag{16}$$

where c_w is the temperature-dependent specific heat of water (J kg^{-1} °C^{-1}), ρ_w is the temperature-dependent fluid density (kg m^{-3}), θ is the porosity (dimensionless), v_x is the groundwater velocity (m s^{-1}), g is the acceleration of gravity (m s^{-2}) and Δh is the change in hydraulic head across the system (ME denotes mechanical energy). The negative sign for the ME conversion term indicates that a decrease in hydraulic head (negative Δh) results in an increase in temperature. Rearranging Eq. (16), we obtain

$$\frac{T_o - T_i}{\Delta h} = \frac{\Delta T}{\Delta h} = -\frac{g}{c_w} \tag{17}$$

Substituting a value of 4186 J kg^{-1} °C^{-1} for c_w, we determine that the temperature should increase by 0.00234°C for every meter drop in hydraulic head or 2.34°C for every 1000 m. This value is the same as that provided by Manga and Kirchner (2004). To put this value into perspective, for the Eastern Snake River Plain, hydraulic head decreases by as much as 870 m from the northeast to the southwest suggesting that the temperature of the infiltrating water should increase by 2.0°C over the length of the plain as a result of viscous dissipation. This result is similar to that obtained by Burns et al. (2016) using an analytical solution for viscous dissipation that they had derived.

In our heat flow simulations, viscous dissipation can be included by equating it with heat injection via an injection well by

$$\theta \rho_w g \left[v_x (\Delta_x h) A_x + v_y (\Delta_y h) A_y + v_z (\Delta_z h) A_z \right] = Q_w c_w \rho_w T \tag{18}$$

where Q_w is an arbitrarily small rate of injection, $\Delta_i h$ is the head difference in the ith direction, and A_i is the area of the cell normal to the ith direction. Eq. (24) can be rearranged to

$$Q_w T = \frac{\theta g}{c_w} \left[v_x (\Delta_x h) A_x + v_y (\Delta_y h) A_y + v_z (\Delta_z h) A_z \right] \tag{19}$$

Thus, from the arbitrary value of Q_w, Eq. (25) can be used to calculate the temperature of the injected fluid, needed to represent viscous dissipation in the aquifer. If a cell already has an injection well, then an energy balance requires that

$$Q_w c_w \rho_w T_{inj} + \theta \rho_w g \left[v_x (\Delta_x h) A_x + v_y (\Delta_y h) A_y + v_z (\Delta_z h) A_z \right] = Q_w c_w \rho_w T \tag{20}$$

where T_{inj} is the temperature of the injected fluid for the existing well and T is the model temperature that is to be used. Solving for T, we obtain to

$$T = T_{inj} + \frac{\theta g}{Q_w c_w} \left[v_x (\Delta_x h) A_x + v_y (\Delta_y h) A_y + v_z (\Delta_z h) A_z \right] \tag{21}$$

3.2 Model Construction

To include vertical heat transport effects in our modes, we started by developing a 10-layer model based on the existing ESPAM model. In particular, the transmissivity is conserved between the multilayer model and the single-layer ESRA model and the wells rates are conserved by placing all of them in the top layer. The components for constructing this multilayer model are described in the following paragraphs.

The aquifer bottom was digitized from the maps provided by Whitehead. Elevations ranged from ~412 m to over 1700 m (Figure 2). As pointed out by Wylie (2004), there are some difficulties with the bottom elevations in the southwest being above ground surface, so

minor adjustments were made to keep the bottom elevation below ground surface. The top of the aquifer was taken to be the elevation of the hydraulic-head surface of the 2-D ESPAM model (Figure 1). The resulting isopach map is provided in Figure 3.

To calculate the heat loss through the top of the aquifer, we used the mean annual air temperature as a boundary condition for the ground surface. The mean annual air temperatures were obtained using Prism-based climate data (Daly et al., 1994). Heat flux through the vadose zone was assumed to be vertical, and dependent on its thickness, thermal conductivity and temperature difference between the water table and the ground surface. A vadose zone thickness map (Figure 4) was constructed by the difference between the topographic elevation and the elevation of the top of the aquifer. The heat loss from the top of the aquifer is simulated using both a first-order decay reaction and a recharge term. The first-order reaction coefficient is defined by Eq. (12) and its distribution is illustrated in Figure 5. For the zeroth-order term, we used an arbitrarily small uniform recharge rate and calculated the temperature of that recharge based on Eq.(8). It is important to understand that this is not are "real" recharge term. That term was included in the well package and we can use it because the recharge package was not used in the ESPAM model. This "theoretical" recharge and its associated temperature are only meant to provide an energy balance that allows heat loss by diffusion through the vadose zone.

For the heat flow through the bottom of the aquifer, we used a total flow into the aquifer equal to 10^{-5} times the total flow through the aquifer system (so as to minimize the impact to the fluid mass balance) and divided the rate by the number of active cells in the bottom layer and injected this fluid in the bottom layer. The associated temperature of this injected water was then calculated using Eq. (5) in order to achieve a heat flow of 100 mW m^{-2}.

Figure 2. Aquifer bottom elevations used in the heat transport model. Taken from Whitehead (1986). Units are in meters.

For the heat flow through the bottom of the aquifer, we used a total flow into the aquifer equal to 10^{-5} times the total flow through the aquifer system (so as to minimize the impact to the fluid mass balance) and divided the rate by the number of active cells in the bottom layer and injected this fluid in the bottom layer. The associated temperature of this injected water was then calculated using Eq. (5) in order to achieve a heat flow of 100 mW m^{-2}.

The grid that was used in the heat transport model is similar to that used in the ESPAM in that it consists of cells that are 1 mile on each side with 104 rows and 209 columns but instead of only one layer, we used 10 layers. The top layer is 33% of the aquifer thickness at every location and all subsequent (lower) layers are equally divided over the remaining thickness. The transmissivity of each of the layers was obtained by multiplying the transmissivity from the ESPAM by the fraction of the aquifer thickness for that particular layer. This method is equivalent to assuming the hydraulic conductivity is constant over the thickness of the model, although it does vary from cell to cell in the x- and y-directions. This approach preserves the calibrated transmissivity distribution obtained with the ESPAM model. The vertical leakance terms were then calculated using the methods described by Harbaugh et al. (2005). The Ibound array was assumed to be the same in every layer. For the wells, we assumed that all of the water was injected into the top layer. This assumption seemed reasonable given that much of the well injection is really irrigation return and that the top layer occupies the upper 33% of the aquifer.

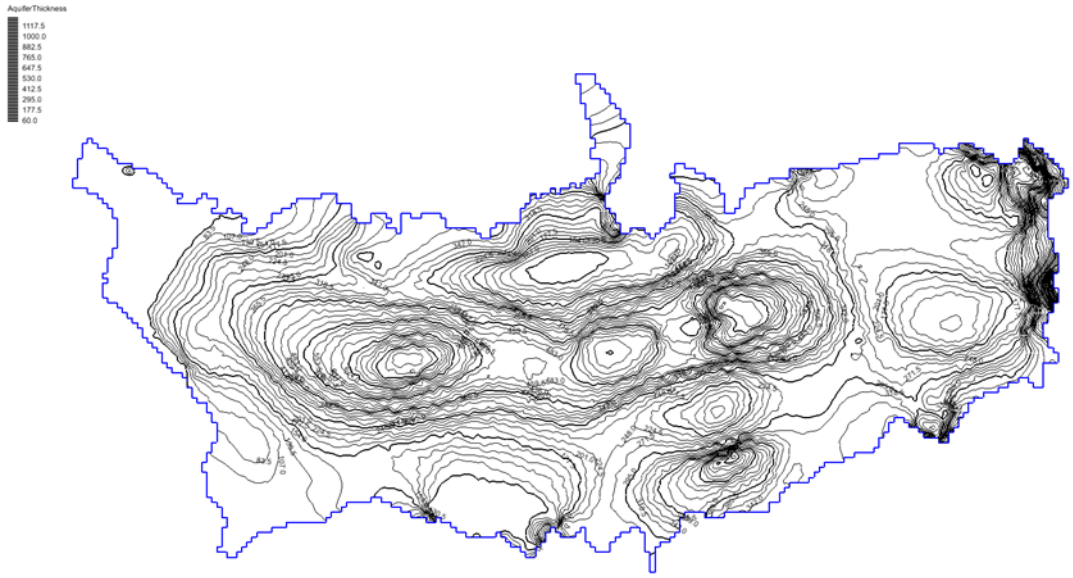

Figure 3. Aquifer thickness. Units are in meters.

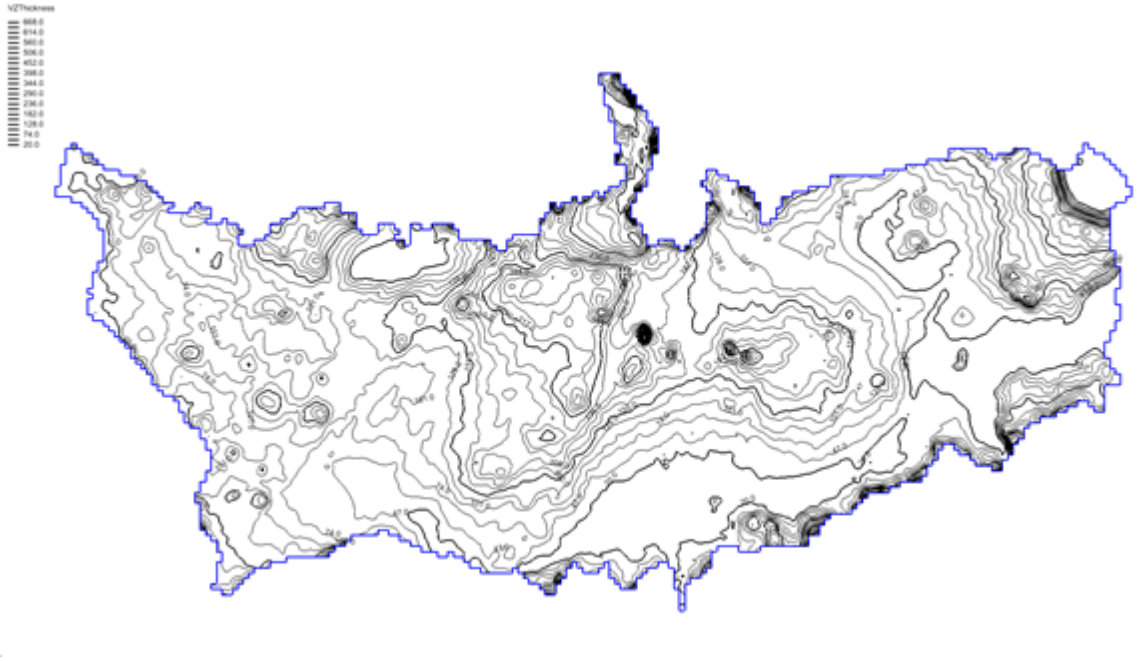

Figure 4. Vadose zone thickness map of the Eastern Snake River Plain. Units are in meters.

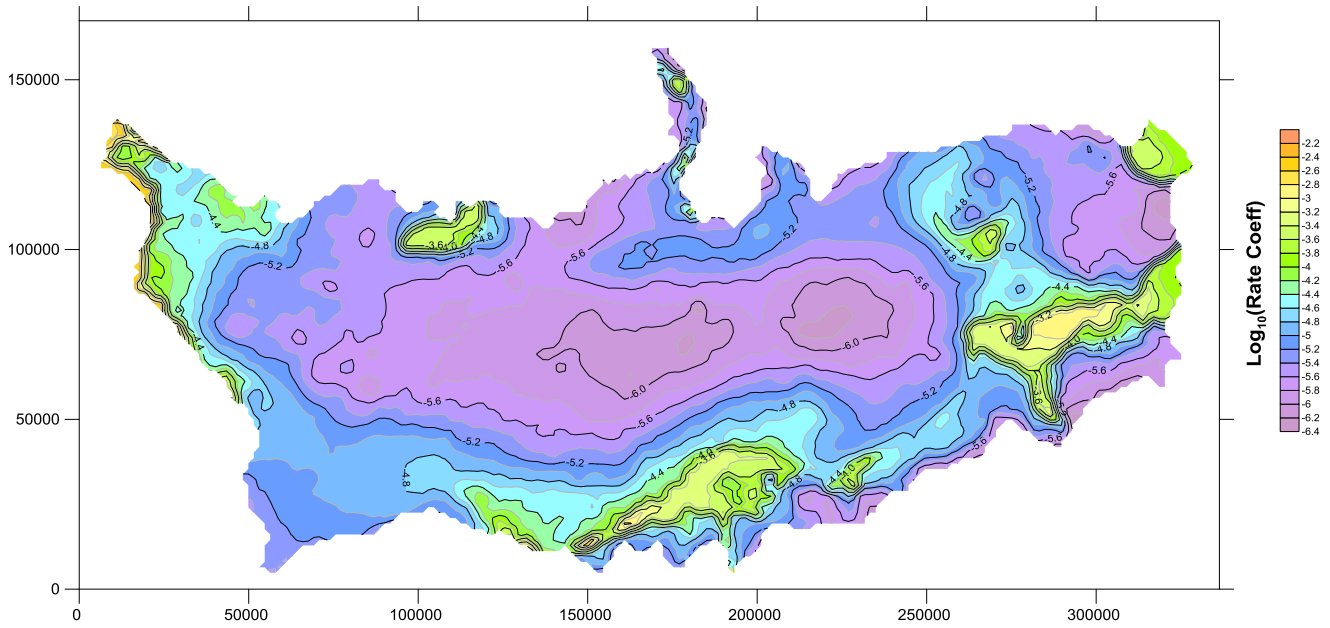

Figure 5. Distribution of the logarithm of the first-order rate coefficient used to simulate heat loss from the top of the aquifer. Units are in log(1/days).

3.3 Thermal Transport Parameters

The Snake River Plain contains several rock types including basalts, rhyolites, and sediments. Rather than account for all of these various rock types, for our initial runs, we assumed a homogeneous system with respect to the thermal properties. This is a reasonable choice given the order of magnitude variation in many of the other relevant parameters compared to the smaller range expected for thermal conductivity and heat capacity. We have chosen thermal transport properties of basalt since this is the dominant rock type in the ESRP.

The thermal conductivity used in the simulations was 1.65 W/(m K). This value is close to the average value of 1.76 ±0.37 W/(m K) reported by Brott et al. (1976). This value is also in the range of mean values of 1.95, 1.69, and 1.45 W/(m K) from three different studies (Schön, 1996); the mean value of 2.11 W/(m K) from 98 samples (Epplebaum, 2014), and 1.69 W/(m K) from Sharma (2002). The specific heat capacity of basalt was taken from the equation of Waples and Waples (2004) which is based on the work of Robertson and Hemingway (1995). At 15ºC the specific heat capacity is 718.7 J kg^{-1} s^{-1}. Using this specific heat capacity and the thermal conductivity discussed in the previous paragraph, we compute the thermal diffusivity to be 8.01E-7 m^2 s^{-1}.

4. RESULTS

The head distribution calculated in the multilayer model is similar to that obtained in the single layer ESPAM model. The key differences are in the extreme northeast corner and the area slightly south of there. The heads in these area are lower than expected and may be the result of the large increase in aquifer thickness over a relatively small distance in these areas. Based on these results, we conclude that the multilayer model adequately represents the head distribution as determined with the ESPAM model.

The temperature distribution in the top layer (layer 1) and the bottom layer (10) are provided in Figure 6 and Figure 7, respectively. A cross-sectional view along row 52 (in the middle of the grid) is provided in Figure 8. These temperature distributions can be compared to kriged measured temperatures which are provided by Welhan (2016) and included as Figure 9. There is general agreement between the temperature range obtained with the heat flow model (5.8 – 30.1ºC) and the kriged values. (< 10 - 34ºC). While the upper layer temperatures seem to reproduce the higher temperatures along the southwest side of the aquifer, other features such as higher temperatures along the "axial thermal high" seen in Figure 9, appear to be missing. However, the deeper portion of the aquifer (Figure 7) appears to show the axial high as well as elevated temperatures in the northeast and long the central portion of the northern boundary. The simulation also shows elevated temperatures in layer 10 between the north western corner and the north-central portion of the aquifer (~19ºC) that is not seen in the kriged map. Figure 9, however, does not include any data in the area.

The cross-section view along row 52 (Figure 8) clearly shows vertical temperature gradients in the aquifer. Where the aquifer is thickest, the 11ºC temperature contour plunges deep into the aquifer.

We urge caution in interpreting differences between aquifer temperature measurements and the simulated results obtained in the heat flow model. In particular, the kriged temperature measurements neglect vertical temperature variation even though vertical temperature gradients are known to exist in the aquifer. Also, as we have seen, little, or no, temperature data are available in some areas of the plain.

Nonetheless, we believe that the results show that the model produces a reasonable match to the 2D variation of temperature in the aquifer. Additional calibration will be required to develop greater confidence in the model.

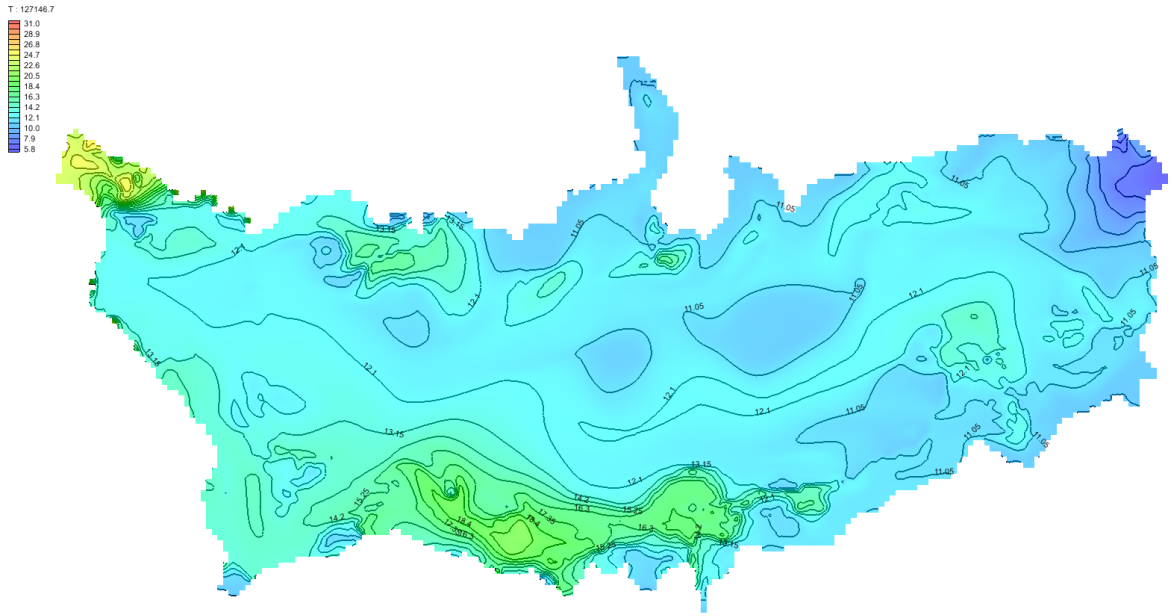

Figure 6. Calculated temperature distribution in the top layer of the aquifer. Units are in ^{o}C.

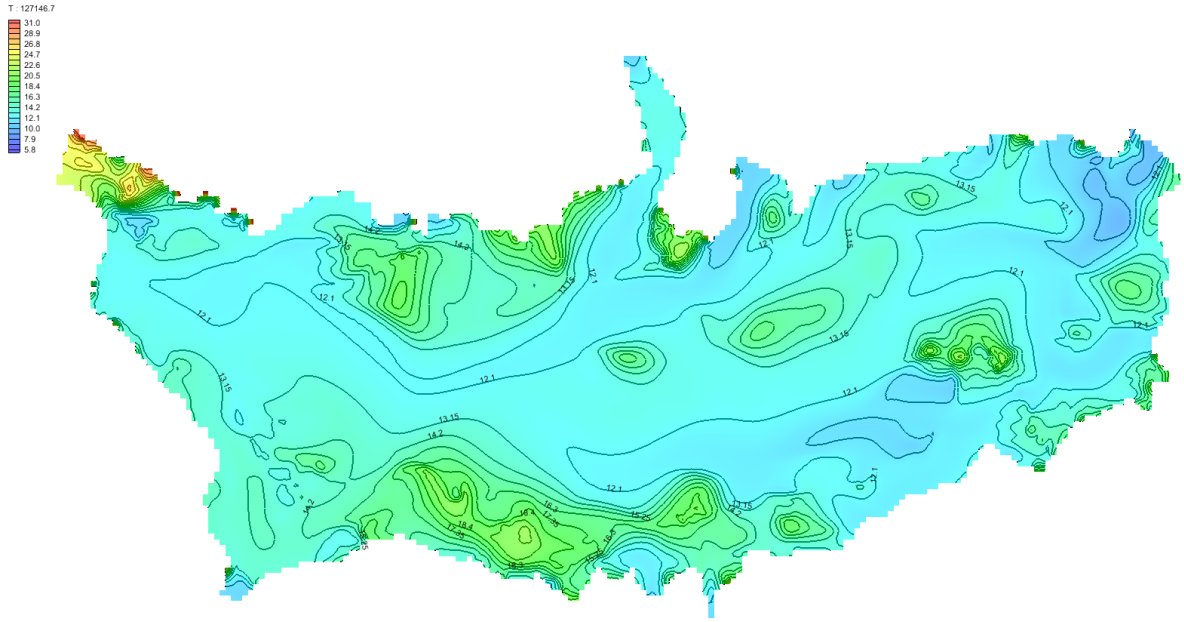

Figure 7. Calculated temperature distribution in the bottom layer of the aquifer. Units are in ^{o}C.

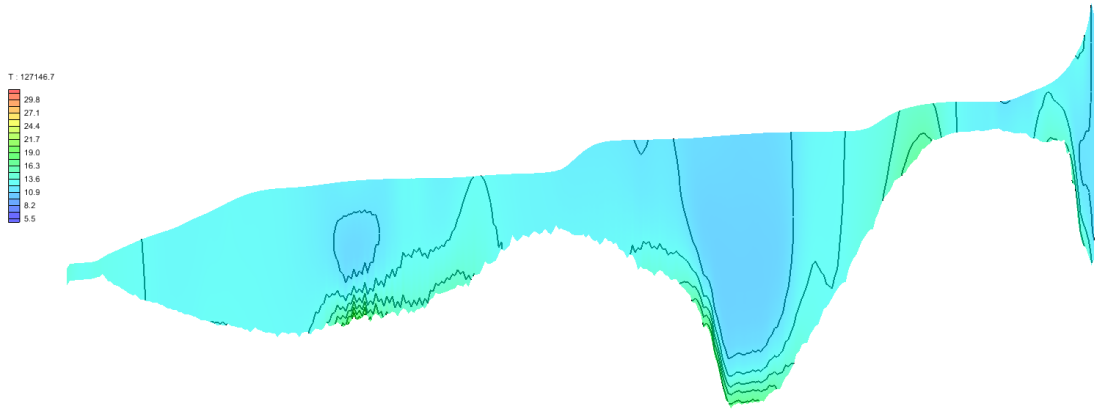

Figure 8. Temperature distributions along row 52. The vertical exaggeration is 100.

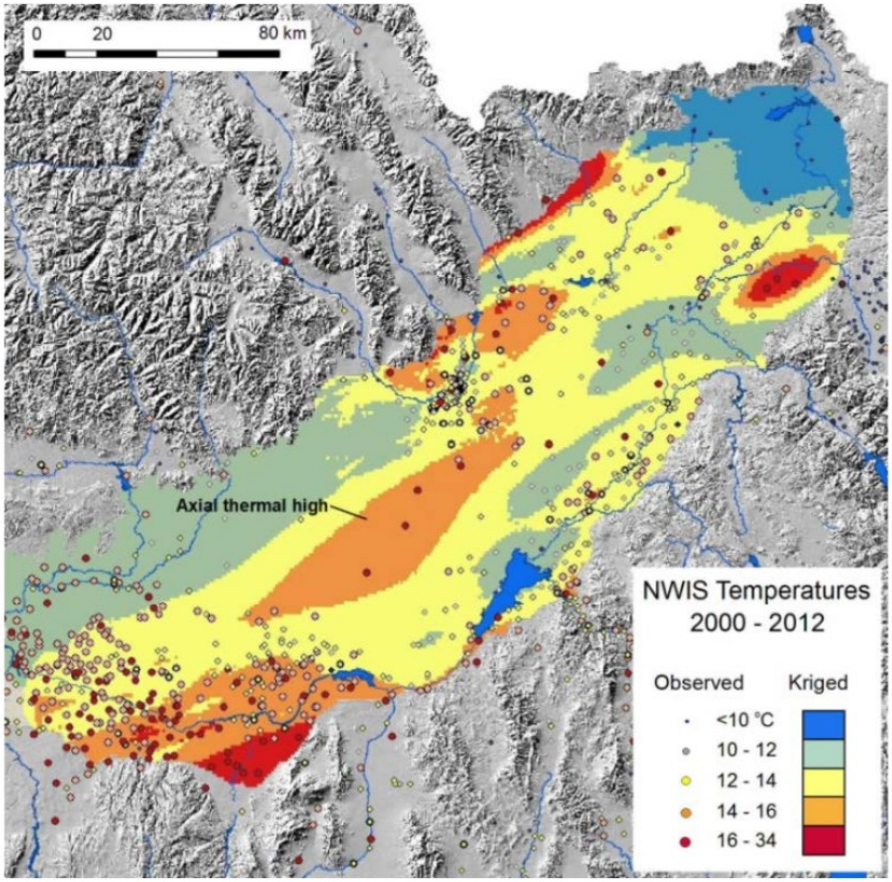

Figure 9. Kriged temperature distributions for the Eastern Snake River Plain. (Welhan 2015).

5. CONCLUSIONS

A thermal transport model of the Eastern Snake River Plain has been developed. The groundwater flow portion of the model is based on the two-dimensional ESPAM model which has been calibrated and appears to represent the aquifer system quite well. We expanded this model to a multilayer model that successfully reproduces the head values. Heat flow was simulated using MT3DMS by altering the solute transport parameters to mimic heat flow parameters. Thermal properties were based on literature values as well as measurement taken at the INL site. The model reasonably reproduces measured temperatures in the Eastern Snake River Plain aquifer. We are

currently adding viscous dissipation effects to the model. The heat transport model developed in this study will be a useful tool for improving our understanding of heat flow in the Eastern Snake River Plain.

REFERENCES

Brott, C.A., Blackwell, D.D., Mitchell, J.C., Geothermal Investigations in Idaho, Part 8, Heat Flow Study of the Snake River Plain Region, Idaho. *Water Information Bulletin* 30, (1976), 207.

Burns, E. R., Ingebritsen, S. E., Manga, M. and Williams, C. F., Evaluating geothermal and hydrogeologic controls on regional groundwater temperature distribution. *Water Resources Research*. Accepted Author Manuscript. doi:10.1002/2015WR018204 (2016)

Cosgrove, D. M., B. A. Contor, and G. S. Johnson, Enhanced Snake River Plain Aquifer Model Final Report," Idaho Water Resources Research Institute, University of Idaho, prepared for the Idaho Department of Water Resources, *IWRRI Technical Report 06-002*, July, (2006).

Daly, C., R.P. Neilson, and D.L. Phillips, A statistical-topographic model for mapping climatological precipitation over mountainous terrain. *J. Appl. Meteor*., 33, (1994) 140-158.

Eppelbaum, L., Kutasov, I., Pilchin, A.: Lecture Notes in Earth System Sciences, *Applied Geothermics,* Springer-Verlag, Berlin Heidelberg, (2014).

Freeze, R.A., Cherry, J.A., *Groundwater*. Prentice-Hall, Inc. (1979).

Harbaugh, A.W., MODFLOW-2005, The U.S. Geological Survey modular ground-water model—the Ground-Water Flow Process: *U.S. Geological Survey Techniques and Methods 6-A16*, variously p. (2005).

Manga, M., Kirchner, J.W., 2004. Interpreting the temperature of water at cold springs and the importance of gravitational potential energy. *Water Resources Research*, 40, W05110, doi:10.1029/2003WR002905, 8 p. (2004).

Robertson, E. C., and Hemingway, B. S., 1995, Heat capacity and heat content of rocks: *U.S. Geol. Survey, Open-File Rept. 95–622*, 38 p.

Schön, J. (1996). *Physical properties of rocks: Fundamentals and principles of petrophysics*. Oxford, OX, UK: Elsevier.

Sharma PV (2002) Environmental and engineering geophysics. Cambridge University Press, Cambridge.

Waples, D.W., Waples, J.S., A Review and Evaluation of Specific Heat Capacities of Rocks, Minerals, and Subsurface Fluids. Part 1: Minerals and Nonporous Rocks. *Natural Resources Research* 13, (2004) 97-122.

Welhan, J.A., Thermal and geochemical anomalies in the Eastern Snake River Plain Aquifer: Contributions to a conceptual mod of the Proposed Forge Test Site. *Proceedings, 41st Workshop on Geothermal Reservoir Engineering*, Stanford University, Stanford, California February 22-24 (2016).

Whitehead, R.L., 1986, Geohydrologic framework of the Snake River Plain, Idaho and eastern Oregon: *U.S. Geological Survey Hydrologic Investigations Atlas HA-681*, scale 1:1,000,000, 2 sheets.

Wood et al. Operable Unit 10-08 Development Report on the Idaho National Laboratory Site Wide Three-Dimensional Aquifer Model. *Report INL/EXT-07-13337*, Idaho National Laboratory and Idaho Cleanup Project, Idaho Falls, Idaho (2007).

Wylie, A., Delineating the Bottom of the Aquifer. *Technical Report 04-015*, Idaho Water Resources Research Institute, University of Idaho (2004)